Efficient and tunable liquid crystal random laser based on plasmonic-enhanced FRET

Guangyin Qu ; Xiaojuan Zhang; Liang Lu ; Siqi Li; Wenyu Du; Zhigang Cao; Chao Li ; Lin Zhang; Kaiming Zhou; Si Wu; Jiajun Ma; Jiangang Gao ; Benli Yu; Zhijia Hu ✉

Check for updates

CrossMark

View Online

Export Citation

Efficient and tunable liquid crystal random laser based on plasmonic-enhanced FRET

View Online   Export Citation   CrossMark

Guangyin Qu,[1] (ID) Xiaojuan Zhang,[1] Liang Lu,[1] (ID) Siqi Li,[1] Wenyu Du,[1] Zhigang Cao,[1] Chao Li,[1] (ID) Lin Zhang,[2] Kaiming Zhou,[2] Si Wu,[3] Jiajun Ma,[4] Jiangang Gao,[5] (ID) Benli Yu,[1] and Zhijia Hu[1,a] (ID)

AFFILIATIONS

[1] Information Materials and Intelligent Sensing Laboratory of Anhui Province, Key Laboratory of Opto-Electronic Information Acquisition and Manipulation of Ministry of Education, School of Physics and Optoelectronic Engineering, Anhui University, Hefei 230601, Anhui, People's Republic of China

[2] Aston Institute of Photonic Technologies, Aston University, Birmingham B4 7ET, United Kingdom

[3] CAS Key Laboratory of Soft Matter Chemistry, Hefei National Laboratory for Physical Sciences at the Microscale, Department of Polymer Science and Engineering, University of Science and Technology of China, Hefei 230026, Anhui, People's Republic of China

[4] The State Key Laboratory of Environment Friendly Energy Materials, Southwest University of Science and Technology, Mianyang 621000, China

[5] Department of Polymeric Materials and Engineering, School of Biological and Chemical Engineering, Anhui Polytechnic University, Wuhu 241000, Anhui, People's Republic of China

[a] Author to whom correspondence should be addressed: zhijiahu@ahu.edu.cn

ABSTRACT

Random lasers (RLs), which possess peculiar advantages (e.g., emission and coherence tunable) over traditional lasers with optical resonators, have witnessed rapid development in the past decades. However, it is still a challenge to tune the lasing peak of an RL over a wide range. Here, a temperature-dependent Förster resonance energy transfer (FRET) RL is demonstrated in pyrromethene 597 (PM597, "donor") and Nile blue (NB, "acceptor") doped chiral liquid crystals. By changing the temperature that drives the liquid crystal bandgap shift, our RL device exhibits a lasing output change from 560 nm (yellow) to 700 nm (red). While the intrinsic FRET efficiency between PM597 and NB is relatively low, the red lasing is weak. By introducing gold nanorods (GNRs) into these RL devices and utilizing GNRs' localized surface plasmon resonance (LSPR) effect, the efficiency of FRET transfer is increased by 68.9%, thereby reducing the threshold of the RL devices. By tuning the longitudinal LSPR to match the emission wavelength of NB, the best 200-fold lasing intensity enhancement is recorded. Our findings open a pathway toward realizing LSPR-enhanced FRET tunable RLs and broaden the range of their possible exploration in photonics research and technologies.

I. INTRODUCTION

Random lasers (RLs), which realize optical feedback in disordered systems, have attracted increasing attention recently.[1–6] In contrast to conventional lasers, RLs have unique superiorities including a simple structure, easy manufacture, low spatial coherence, and output wavelength tunability.[7,8] Among these properties, wavelength tunability is an important feature that profoundly affects and determines the application scope of laser devices. As for tuning

the output wavelength in traditional lasers, people have to change the resonant frequency (or wavelength) of the resonant cavity and the optical mode of the lasing emission. For RLs, the lack of a well-defined resonator makes it relatively easier to tune the lasing emission. To date, two major approaches have been suggested to tune RLs' emission wavelengths. One approach to change the emission wavelength of gain materials via external stimuli. For instance, Xu et al.[9] proposed a wavelength-tunable RL based on densely packed metal-organic framework particles embedded with

intramolecular charge transfer laser dyes, in which the energy levels of organic gain molecules can be effectively modulated via thermal stimuli. Another alternative approach is to tune the resonance of the scatters. Gottardo *et al.*[10] showed that the Mie resonance of microspheres can be used to adjust the output wavelength of RLs, where the resonance wavelength is strictly dependent on the particle size and refractive index of the sphere. Recently, Shi *et al.*[11] proposed a spectral encryption method based on the selective visualization of spectral patterns in RLs. By coupling with the external whispering gallery mode cavity, hidden localized lasing modes with special multiple-peak spectra were selected from phase-correlated RLs with smooth single-peak spectra.

Nevertheless, there are obvious drawbacks to these methods of changing lasing wavelengths. These approaches not only suffer from technical difficulties in fabricating the desirable structures but also lack a wide wavelength regulation range.[12,13] In this paper, we report an exploit that uses liquid crystal (LC) with a temperature-sensitive bandgap to achieve a wide range of laser wavelength control. LC materials with the unique anisotropy of birefringence are widely used as disordered media to generate RLs.[14–17] The feedback from the lasing comes from the multiple scattering of photons between LC boundaries. LC molecules have different responses to external temperature[18–23] and electric field,[24–28] which provides the possibility of tuning the LC-based RLs emission when exerting exterior temperature or electric field. Wiersma and Cavalieri[29] have successfully demonstrated controlling the laser radiation characteristics of dye-doped LC RLs by changing temperature. During temperature change, the LC transforms from nematic to isotropic states, which increases the lasing radiation bandwidth and reduces the radiation intensity. Here, we incorporate two dyes, pyrromethene 597 (PM597) and Nile blue (NB), which emit at around 568 and 680 nm, respectively, into LC structures. Such a mixture will ensure a broad emission range as the substrate waits for further LCs' bandgap coupling. While the absorption spectrum of NB is far from the

laser band of the pumping laser source wavelength in our experiment (532 nm nanosecond laser), NB cannot be directly excited by the pumping laser source. A Förster resonance energy transfer (FRET) system with the donor PM597 as a bridge needs to be established using a laser with a 532 nm wavelength. Based on such a FRET mechanism, an emission tunable RL from 560 to 700 nm was fabricated utilizing the temperature-dependent chiral liquid crystal (CLC) bandgap change [Fig. 1(a)].

However, it should be noted that FRET's efficiency in such a system is not high, and the laser's emission intensity at a long wavelength (stimulated emission of NB) is low. Therefore, we consider introducing plasmonic nanoparticles into the system to improve the transfer efficiency and boost laser emission intensity at long wavelengths. The free electrons of plasmonic nanostructures will oscillate under the excitation of the external electromagnetic field. When the frequency of electron collaborative oscillation is close to the frequency of an incident light wave, localized surface plasmon resonance (LSPR) will be generated. The LSPR effect has been widely applied in surface-enhanced Raman spectroscopy (SERS),[30,31] surface-enhanced fluorescence,[32–34] plasmonic micro/nano-lasers,[35–38] and plasmonic RLs.[39] The threshold of RL is usually reduced after incorporating plasmonic nanoparticles.[40] Besides, plasmonic NPs can also work as scatters in RLs, as they can scatter light much more strongly than their dielectric counterparts of the same size, especially at the plasmon resonant wavelength.

Here, we selected gold nanorods (GNRs), which are common plasmonic NPs that possess two prominent LSPRs, transverse and longitudinal modes. The longitudinal LSPR is length-diameter ratio-dependent, providing an easy method to select preferred plasmonic resonances by changing their ratios. After polyvinyl pyrrolidone (PVP-K90) surface modification, we successfully added hydrophilic GNRs to PM597 and NB doped CLCs. By adjusting their longitudinal LSPR to approach the center wavelength of NB's emission (700 nm), the FRET efficiency is significantly boosted. The device's
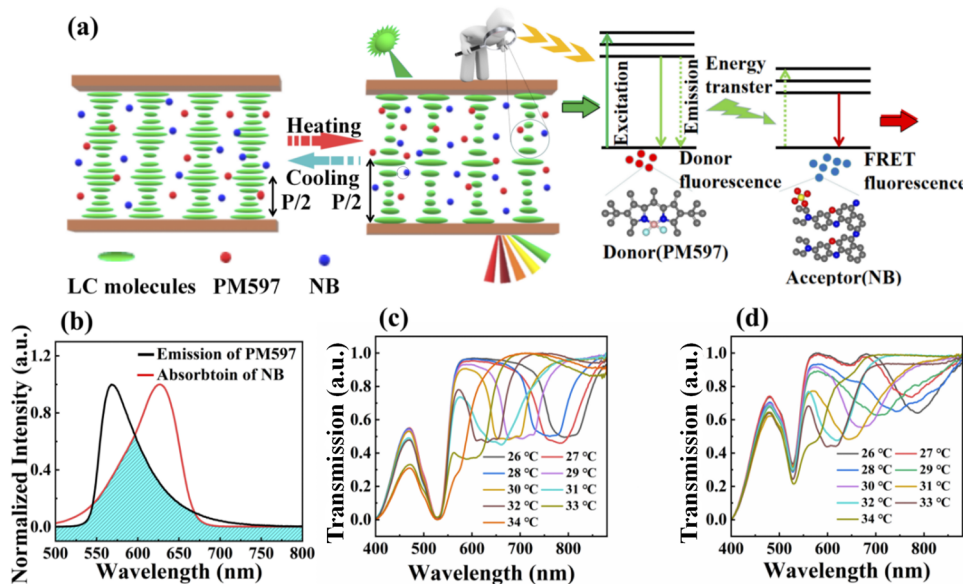
FIG. 1. The basic spectrum of the FRET process and the analysis of the optical properties of the sample. (a) Schematic illustration of helical structures for cholesteric phases. In this configuration, the helical axis is perpendicular to the substrates. (b) Absorption spectra of NB dye and emission spectra of PM597 dye. The green shade represents spectral overlap, which is the basis of the FRET system. Transmission spectra of (c) PM597 doped LCs and (d) PM597 and NB doped LCs at different temperatures.

lasing threshold decreases correspondingly, and a best red lasing intensity increment of two orders of magnitude is observed.

II. RESULTS AND DISCUSSION

A. The optical physics basis of random laser energy transfer

FRET is widely used to study the molecular level interaction, quantitative measure of chromophore distance, structures, and dynamics of macromolecules and molecules.[41] Another application of FRET is in dye lasers.[42] FRET can be defined as a process of energy transfer between two molecules, one of which is an energy donor and the other an energy acceptor. The energy transfer does not occur due to donor emission and acceptor absorption but by charge-charge interaction between oscillating donor and acceptor dipoles nearby.[43,44]

The FRET efficiency E can be expressed in terms of two rate constants. These relate to the fluorescence lifetime of the donor in the absence of the acceptor ($k_D = \tau D^{-1}$) and the energy transfer rate between the donor and the acceptor (k_T). E is hence easily determined by comparing the fluorescence lifetimes τD of the donor only species and $\tau_T^{-1} = k_D + k_T = \tau_D^{-1} + k_T$ for the donor-acceptor species.[45]

The gain material in the FRET system consists of two laser dyes: PM597 acting as the donor and NB acting as the acceptor. In our research, the mass fraction of PM597 (NB, PM597/NB) is kept at 1%. In order to characterize the basic optical properties of the selected dyes, the absorption in ethanol solution and fluorescence spectra in CLC (30% S811 and 70% E7, mass fraction) of the donor dye (PM597), the accepted dye (NB), and the mixed dye (PM597/NB) were characterized. As shown in supplementary material, Fig. 1a, PM597/NB mixture material presents two wide absorption peaks, which correspond to the absorption peaks of dye PM597 and NB, respectively. supplementary material, Fig. 1b, shows the emission spectra of the dyestuffs PM597, NB, and PM597/NB mixture. It is interesting to find that there is only one emission peak in the PM597/NB mixture at 693 nm, which matches the emission peak of the NB dye. This is because the donor dye PM597 transfers its energy efficiently to the nearby recipient dye NB via FRET rather than emitting fluorescence. The results confirm that the PM597/NB dye mixture is an ideal gain medium for the FRET system. To explain the role of PM597 and NB in the FRET system, the emission spectra of the laser dye PM597 are compared with the absorption spectra of the laser dye NB [Fig. 1(b)]. It shows that the two spectra overlap well in the wavelength range of 550–650 nm, ensuring the energy transfer process from the donor dye (PM597) in the excited state to effectively excite NB in the ground state. It is worth noting that the absorption spectrum of NB is far from the 532 nm pumped laser source, which results in the fact that it cannot be directly excited by the pumped laser and must be bridged by FRET from the donor dye to achieve long-wavelength random laser emission.

Figures 1(c) and 1(d) represent the transmission spectra of samples E7+S811+PM597 and E7+S811+PM597+NB at different temperatures. The dip at the wavelength of 532 nm in every transmission spectrum results from the absorption of the dye PM597. It can be seen that there is no selective reflection band in the spectra with a temperature below 27 °C. As the temperature exceeds 27 °C, the selective reflection band appears in the near-infrared

region, and the blue-shift effect occurs with increasing temperature continuously. When the temperature reaches 36 °C, the reflection band gradually stabilizes at about 500 nm. It can be observed from Figs. 1(c) and 1(d) that the bandwidth of reflection becomes narrower during blue-shift, which can be explained by the formula $\lambda_C = n \times P$. The selective reflection band is centered at the wavelength λ_C, with the width of the band given by $\Delta\lambda = (\Delta n/n) \lambda_C$, where $\Delta\lambda$ is the bandwidth of the bandgap, P is the pitch of the CLC, and $n = (n_{e} + n_{o})/2$ the average refractive index of the cholesteric planes having a birefringence of $\Delta n = n_{e} - n_{o}$, with n_e and n_o being the extraordinary and ordinary refractive indices of the nematic LC, respectively.[46] When the external temperature changes, the internal pitch [Fig. 1(a)] and average refractive index of the CLC change. This temperature sensitivity allows the CLC reflection band to be modulated by external temperature stimuli. As can be seen from the formula, with the wavelength blue shift, the CLC pitch becomes smaller, and the bandwidth of the reflection band becomes narrower. Similarly, the transmission spectra of samples E7+S811 and E7+S811+NB in the supplementary material, Fig. 2, also obtain consistent results.

To investigate the changes in the fine structure of the LC phase at different temperatures, we observed the polarizing microscope (POM) photos of samples E7+S811, E7+S811+PM597, and E7+S811+PM597+NB at different temperatures (Fig. 2). When the sample is at room temperature (~25 °C), the LC is in a near-crystal A state, and its structure and texture are shown in the supplementary material, Fig. 3c. As can be seen from Fig. 2(b), when the temperature rises to 28.500 °C, it shows a typical cholesteric oily streak texture. Furthermore, when the temperature reaches 35.520 °C, the oil filament texture breaks. Since the free energy of LC molecules is the same after fracture, the LC molecules tend to aggregate so that the cross-linking between the fracture points can be re-linked. Such fracture points may be relatively weak, and if the temperature continues to increase, multiple fracture points tend to accumulate. Due to the interaction of surface tension and large amounts of heat within the LC, this irregular fracture gradually increases, eventually forming a "circular" black hole. The black hole gradually erodes away
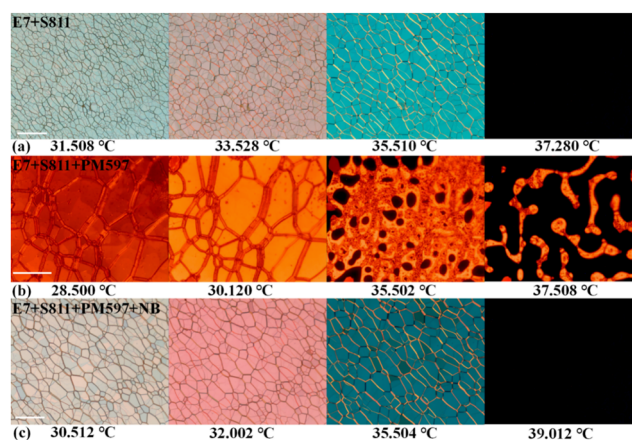
FIG. 2. Photographs of samples at different temperatures under a POM. (a)–(c) Represent POM photos of samples E7+S811, E7+S811+P597, and E7+S811+PM597+NB at different temperatures, respectively. Scale bar: 100 μm.

at the surrounding oily streak and affects the direction of the oily streak. When the temperature is above 37.280 °C [Fig. 2(a)], black holes cover the entire sample. Then, we observed the POM photos of the crystal texture and structure changes in the cooling process. The detailed process is shown in the supplementary material. At different temperatures, LC undergoes an incomplete reversible phase transition, which changes the arrangement of the LC molecules. The spatial refractive index and scattering intensity of LC materials vary with the arrangement of the molecules. The scattering coefficient of the LC decreases with an increase in the temperature inside the sample. When the LC is in the isotropic state, the absorption coefficient of the LC is greater than the scattering coefficient, so the blackening of the field of vision is observed in POM. In addition, as the temperature changes, the bandgap of the LC shifts, leading to changes in the internal refractive index of the material, which makes the sample reflect different colors under POM.

B. Spectral characteristics of the random laser before and after energy transfer

The experimental setup to measure the random lasing emission spectrum of the dye-doped CLC is shown in Fig. 3(a). One pumped laser beam is derived from a Q-switched Nd:YAG second-harmonic-generation pulse laser (wavelength of 532 nm, pulse duration of 10 ns, and repetition rate of 10 Hz). The pump pulse energy and polarization are controlled by a Glan prism group. The emitted light along the CLC axis is collected by a fiber spectrometer (QE65PRO, Ocean Optics, resolution ~0.4 nm, integration time 100 ms). The diameter of the pump beam on the sample is about 100 μm.

The random lasing spectra of PM597 doped CLCs at different temperatures are shown in Fig. 3(b). When the temperature slowly increases to 27.130 °C, the band edge lasing is observed at a wavelength of 626 nm. As seen from Fig. 3(b), the bandgap lasing is gradually blue-shifted as the temperature increases. When the temperature reaches ~35 °C, a bandgap laser is produced at a wavelength of about 560 nm. The wavelength of the band-gap laser shifts by nearly 70 nm when the temperature increases from 27 to 35 °C. Afterward, we collected the random lasing spectrum changes during the cooling process. As shown in the supplementary material, Fig. 4, it can be concluded that the laser wavelength has a red shift as the temperature decreases. This is because the LC molecules gradually change from the smectic A state to the cholesteric state as the temperature rises to room temperature (~25 °C). The arrangement of LC molecules in the smectic A state is ordered, and the structure of LC molecules in the cholesteric state is partially ordered. Therefore, the scattering of the LC cholesteric phase is stronger than that of the smectic A phase. Meanwhile, the bandgap feedback of CLCs also promotes the generation of RLs. When a beam of the pump light is incident on the sample, the planar texture of the CLC causes multiple scattering to form RL emission. In addition, the bandgap feedback in the texture of the CLC results in the emission of a fixed wavelength. Therefore, both effects enhance the adjustable RL in the cholesteric plane texture.[47]

Although we have successfully demonstrated band-gap-tailored RL with a wide tunable range, the limited range of wavelength regulation limits its applications. In order to further broaden the control range of the laser wavelength, we introduced the FRET system. In the FRET system, the laser dye PM597 acts as the donor, and NB acts as the acceptor.
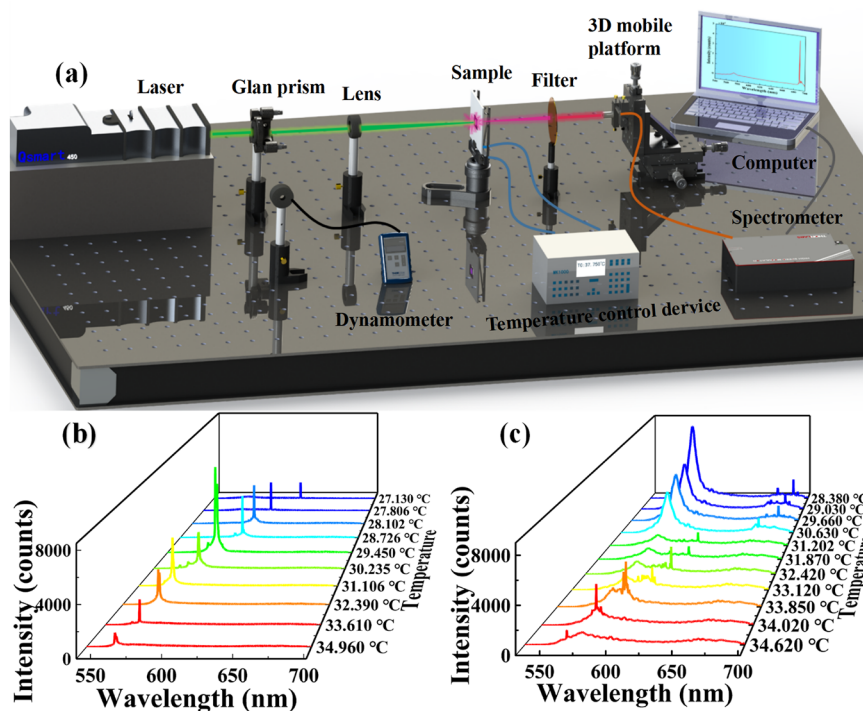
FIG. 3. The spectral characteristics of FRET random laser. (a) Experimental setup for the temperature controlling random laser. (b) Random laser spectra of sample E7+S811+PM597 at different temperatures during the heating process. (c) Emission spectra of FRET-based RLs. PM597: NB, 3/2.

In order to exclude the possibility of lasing from dye NB pumped at 532 nm, we first prepared a control sample, which was doped only with NB (1.0 wt. %) dye at the same concentration as the other samples. As verified in the supplementary material, Fig. 5, no random lasing phenomenon is observed in this control sample due to the low absorption rate of NB dye at 532 nm. Therefore, we rule out the possibility that the laser dye NB itself can be pumped by a 532 nm laser to produce a long wavelength random lasing. To explore the temperature-dependent FRET process, we studied the random lasing spectra of CLC with different PM597/NB mass ratios (PM597/NB = 3/1 and 3/2). As demonstrated in the supplementary material, Fig. 6, when the PM597/NB mass ratio is 3/1, random lasing is observed in the wavelength range of 560–620 nm, while only weak fluorescence peaks are observed in the wavelength range of 660–700 nm.

When the mass ratio of PM597/NB is 3/2, it can be seen in Fig. 3(c) that the lasing peak appears within the wavelength range of 660–700 nm with the change of temperature. However, a strong fluorescence peak was observed within the wavelength range of 560–620 nm, indicating that the high content of PM597 in the system resulted in the low efficiency of FRET. Due to the low transfer efficiency of FRET and the low fluorescence intensity of NB, the intensity of the bandgap lasing emitted in the wavelength range of 660–700 nm is relatively weak.

C. FRET's transfer efficiency is increased by LSPR, which also exactly increases a specific wavelength's laser intensity

For the sample E7+S811+PM597+NB (PM597/NB = 3/2), the intensity of the RL generated is relatively low, which has a certain impact on its application. For this reason, on the basis of wide-range regulation of RL (by introducing GNRs into the system), we selectively enhance RL emission to obtain wide-range and high-efficiency RL emission. It should be noted that, despite the FRET-based emission tuning that has been demonstrated earlier, the FRET efficiency is still low. To boost the FRET efficiency, we consider adopting an enhancement strategy in the current system. It is regarded that adding plasmonic nanostructures, which have the famous LSPR effect to enhance the FRET, is an effective approach. Among the plasmonic nanostructures, GNRs are the "star" nanomaterial since they can be easily synthesized using wet chemistry methods and have excellent stability. The position of the LSPR peak mainly depends on the size, shape, and surface charge of GNRs. GNRs have two distinct surface plasmon formants: one is transverse LSPR, and the other is longitudinal LSPR. Compared with the transverse LSPR (which usually stays fixed at about 520 nm), the longitudinal LSPR has stronger light absorption, with its absorption peak being sensitively dependent on the aspect ratio of GNR. Therefore, we synthesized GNRs with different wavelength absorptions by designing different aspect ratios.[48] The synthesis process is shown in Fig. 4(a), and the detailed process is shown in the supplementary material, Fig. 7. To obtain the longitudinal LSPR peaks at 677, 685, 690, and 695 nm, the synthesized GNRs are designed to have mean lengths and diameters of 62/24, 56/20, 70/25, and 78/27 nm, respectively, as determined by transmission electron microscopy (TEM) [Figs. 4(c)–4(f)]. The size (length, width, aspect ratio) distribution map of GNRs is in the supplementary material, Fig. 8. In addition, the transmission spectra of E7+S811+PM597+NB+GNRs samples at different temperatures are shown in the supplementary material, Fig. 2c.

We added the PVP-modified GNRs to the sample E7+S811+PM597+NB (PM597/NB = 3/2), forming a composite structure [Fig. 4(b)]. The random lasing properties of LSPR-enhanced CLC devices are compared with control samples at room temperature (supplementary material, Fig. 9). The relationship between output intensity and pump intensity is also analyzed, which reveals that the random lasing thresholds of PM597 doped CLC system, PM597/NB doped CLC system, and PM597/NB doped LSPR-enhanced CLC system are 4.0, 2.0, and 1.2 μJ, respectively. Obviously, with the addition of GNRs, the RL threshold is significantly reduced. We suggest that the low-threshold RL is caused by the cooperative effect of recurrent multiple scattering and field enhancement in the vicinity of GNRs. The localized electric field near the GNRs boosts the absorption and transition rate of the
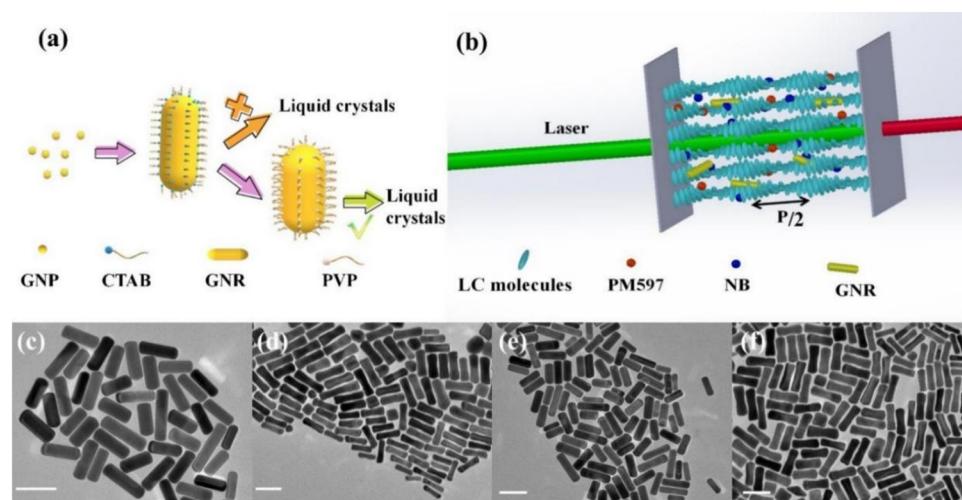
FIG. 4. Synthesis and characterization of GNRs and preparation of samples. (a) The schematic of the synthesized process and PVP modification GNRs. (b) Internal structure of the LC cell. (c)–(f) TEM images of GNRs with aspect ratios of 2.56, 2.67, 2.75, and 2.88, respectively. Scale bar: 50 nm.

dyes near the GNRs (supplementary material, Fig. 10), thereby strengthening the fluorescence amplification and reducing the laser threshold. Moreover, GNRs also work as scattering particles, which are conducive to enhancing scattering and forming feedback for light amplification.

In this system, the GNRs can not only reduce the laser threshold but, more importantly, they can enhance the FRET efficiency of the system. The efficiency of FRET (E) is calculated by measuring the lifetimes τ_D and τ_{DA},[49]

$$E = 1 - \tau_{DA}/\tau_D.$$

In which τ_D is the fluorescence lifetime of donors in the absence of the acceptor, and τ_{DA} is that of donors in the presence of an acceptor. We performed PL lifetime tests on four samples containing PM597, PM597+GNRs, PM597+NB, and PM597+NB+GNRs, as shown in the supplementary material, Fig. 9. The lifetimes of different samples are shown in the supplementary material, Table 1. According to the formula, the FRET transfer efficiencies with or without GNRs in the system were calculated to be 20.9% and 35.3%, respectively. The FRET efficiency can be improved by 68.9% due to the introduction of GNRs in the system. This is because fluorophores near the plasmonic nanostructures would experience excitation rate enhancement, emission rate enhancement, and thus enhanced FRET efficiency.

In order to accurately enhance the random lasing at a certain wavelength, we use GNRs with different longitudinal LSPRs to
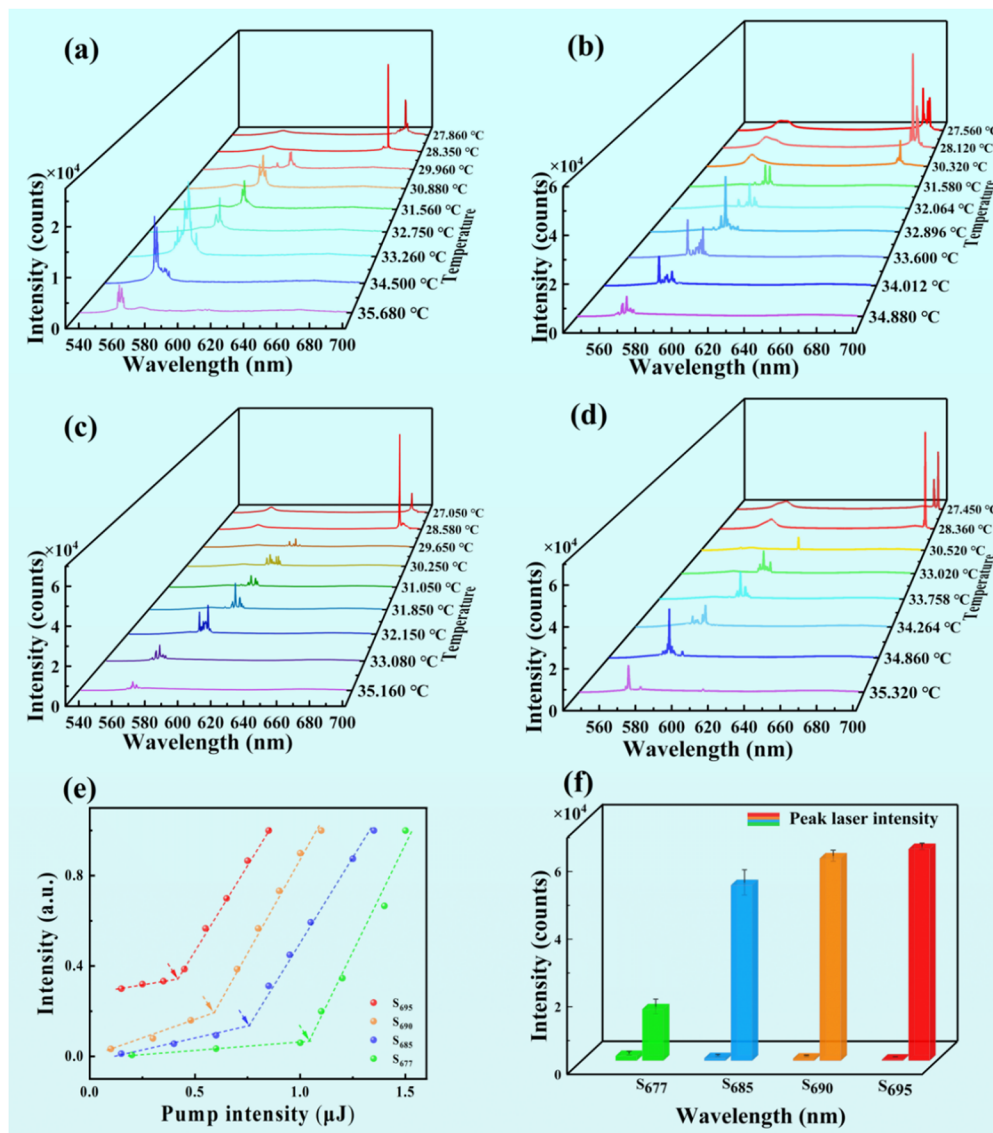
FIG. 5. Random laser spectra of the sample. (a)–(d) Represent the laser spectra of samples S_{677}, S_{685}, S_{690}, and S_{695} at different temperatures, respectively. (e) The threshold of the corresponding sample. (f) Strength comparison before and after GNRs addition.

control and enhance the lasing. Four GNRs with different aspect ratios were added to the sample. Four sets of samples are named S_{677}, S_{685}, S_{690}, and S_{695}, respectively (where the values represent the spectral position of longitudinal LSPR). The RL spectra at different temperatures of these samples are shown in Fig. 5, and it can be seen that the RL blue shifts with the increase in temperature. This is consistent with the results obtained in the supplementary material, Fig. 5. The blue shift is mainly due to the multiple scattering of the CLC and the bandgap feedback of the LC, resulting in the emission of a fixed wavelength. Compared with Fig. 3(c), it can be seen that with the addition of GNRs, the intensity of laser emission is markedly increased, and the transfer efficiency of FRET is also significantly improved.

As can be seen from Figs. 5(a)–5(d), the addition of GNRs significantly enhanced the lasing intensity of samples S_{677}, S_{685}, S_{690}, and S_{695} at wavelengths of 677, 685, 690, and 695 nm. Combined with the supplementary material, Fig. 11, these values correspond to the LSPR positions of these GNRs. The thresholds of S_{677}, S_{685}, S_{690}, and S_{695} were 1.1, 0.72, 0.60, and 0.45 μJ, respectively [Fig. 5(e)]. Therefore, we have successfully prepared a low-threshold RL with wide-range regulation, high-efficiency emission, and control of emission wavelength.

Figure 5(f) is the random lasing intensity comparison before and after adding GNRs. It can be seen that random lasing intensity is increased by 11.2, 73.5, 101, and 200 times for samples S_{677}, S_{685}, S_{690}, and S_{695}, respectively. The maximum enhanced factor of sample S_{695} is mainly caused by the large overlap between the fluorescence peak of 693 nm (supplementary material, Fig. 1b) for the mixed dyes and the LSPR of 695 nm for GNRs. Therefore, at $\lambda_{LSPR} \approx \lambda_{Em}$, the fluorescence molecule can obtain the maximum emission efficiency and greatly improve the laser output intensity. The plasmonic-induced hot electron injection and the plasmonic-induced resonance energy transfer may be involved in the FRET process.[50] To verify the mechanism of the FRET process in RL devices, we coated the GNRs with an 8 nm layer of silica (supplementary material, Fig. 12). Silica coating is a common strategy utilized to regulate or essentially block hot electron transfer to the surrounding environment and has been widely used to distinguish hot electron catalysis from thermal effects in plasmonic catalysts.[51] This silica layer acts as a filter, allowing electromagnetic fields to penetrate but blocking hot electrons from reaching the molecules. Comparing the lasing performance test, we found that the lasing emission intensity of the GNRs with silica coating in the device rose by 191 times at the wavelength of 692 nm (supplementary material, Fig. 13), which is almost similar to the PVP-modified GNRs (192.6 times, λ = 688 nm). Hence, the mechanism of the FRET process in our device system is primarily plasmonic-induced resonance energy transfer. Therefore, the GNRs intrigued by FRET enhancement can be explained by the theory of local electromagnetic field enhancement induced by surface plasmons. The coupling between the GNRs and the incident light makes the free electrons on the surface of the nanorods oscillate collectively, resulting in the LSPR effect, and the electromagnetic field near the nanorods is greatly augmented. While the ability of dyes to absorb and radiate is proportional to the intensity of the electromagnetic field according to Fermi's golden rule. Furthermore, the excitation efficiency of dyes is proportional to the electric field intensity at its location, and the emission of dyes is proportional to the

radiation field.[52] Therefore, the appearance of GNRs can effectively change the absorption and radiation characteristics of the nearby fluorescence molecules, thus increasing their absorption and emission efficiency, improving the efficiency of the optical gain, and thereby enhancing random lasing intensity.[53] In addition, when the dye is in the excited state, it can transfer energy to the nearby local surface plasmons, and then the local surface plasmons radiate the energy to the far field with higher efficiency to improve the fluorescence radiation characteristics.

Speckle noises are considered the most common manifestation of coherent artifacts. Due to the very high spatial coherence of a typical laser diode, the scattered lights can thus interfere with each other and form notable speckles. In random lasers, multiple laser modes from different random cavities are excited simultaneously, significantly reducing the spatial coherence without spoiling the laser intensities. Since the coherence of the RL device is low, we consider applying it to full-field speckle-free imaging. A comparison imaging experiment is implemented using a commercial Nd:YAG laser at 532 nm. Furthermore, due to the low coherence of the RL, we carried out full-field imaging experiments to test the ability of the RL for speckle-free imaging. The RL operating above the threshold and the Nd:YAG laser are used as the light sources to image a resolution test chart, respectively. The speckle contrast value is obtained from the speckle image by using the bandgap laser as the illumination source. The speckle images of the bandgap laser are shown in Fig. 6. The speckle contrast[54] C is defined as $C = \sigma/\langle I \rangle$, where σ is the standard deviation of the speckle intensity and $\langle I \rangle$ is the average intensity of the speckle. The C values for Figs. 6(a)–6(d) are 0.9252, 0.7954, 0.4575, and 0.5472, respectively. The comparison of C values shows that the imaging result of using the RL [Figs. 6(b)–6(d)] is much clearer than that of using the Nd:YAG laser [Fig. 6(a)]. This shows that our RL is an ideal light source for full-field speckle-free imaging applications.
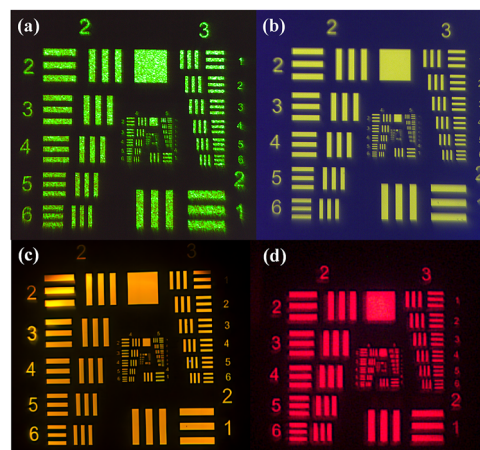
FIG. 6. Optical photographs of the resolution test chart illuminated by (a) a commercial Nd:YAG laser at 532 nm and (b)–(d) by a random laser with emission wavelengths of 580, 610, and 690 nm.

III. CONCLUSION

To summarize, we first obtained a band-gap custom LCRL using FRET-based mixed dyes as gain materials. A wide adjustable range (560–700 nm) is achieved in our RL devices through simple temperature regulation (26–35 °C). For further amplifying the FRET process, GNRs-plasmonic nanoparticles that possess LSPR are introduced. The LSPR will create an augmented electric field that promotes the absorption and emission abilities of dyes near the surface, thereby improving FRET efficiency. A maximum 200-fold lasing intensity is recorded when the longitudinal LSPR of GNRs is overlapped with the emission wavelength of the NB well. We envision that such emission wavelength tunable RLs with low thresholds, as demonstrated in this work, would open a window for RLs' applications in the laser display and optical communication fields. In addition, this plasmonic enhanced FRET strategy is believed to be a novel but universal method to control emission in lasers, light-emitting diodes, and other optoelectronic devices.

SUPPLEMENTARY MATERIAL

See the supplementary material for details on the following aspects: synthesis of GNRs and experimental setups (supplementary material, Sec. I). Absorption and emission spectra of partial laser dyes. Transmission spectra of some samples at different temperatures. Particle size distribution of GNRs and calculation of FRET efficiency for different samples (supplementary material, Sec. II).

AUTHOR DECLARATIONS

Conflict of Interest

The authors declare no conflict of interest.

Author Contributions

Guangyin Qu, Xiaojuan Zhang, and Liang Lu contributed equally to this work.

Guangyin Qu: Conceptualization (equal); Formal analysis (equal); Investigation (equal); Software (equal); Writing – original draft (lead); Writing – review & editing (lead). **Xiaojuan Zhang**: Investigation (equal); Supervision (equal). **Liang Lu**: Conceptualization (equal); Formal analysis (equal). **Siqi Li**: Methodology (equal). **Wenyu Du**: Software (equal). **Zhigang Cao**: Resources (supporting). **Chao Li**: Formal analysis (equal). **Lin Zhang**: Supervision (equal). **Kaiming Zhou**: Formal analysis (equal). **Si Wu**: Resources (supporting). **Jiajun Ma**: Investigation (equal). **Jiangang Gao**: Investigation (supporting); **Benli Yu**: Resources (supporting). **Zhijia Hu**: Formal analysis (equal); Funding acquisition (equal); Project administration (equal); Resources (equal); Supervision (equal).

DATA AVAILABILITY

The data that support the findings of this study are available from the corresponding author upon reasonable request.

REFERENCES

[1] W. Gao, T. Wang, J. Xu, P. Zeng, W. Zhang, Y. Yao, C. Chen, M. Li, and S. F. Yu, "Robust and flexible random lasers using perovskite quantum dots coated nickel foam for speckle-free laser imaging," Small **17**, 2103065 (2021).

[2] X. Jiang and C.M. Soukoulis, "Time dependent theory for random lasers," Phys. Rev. Lett. **85**, 70 (2000).

[3] N. M. Lawandy, R. M. Balachandran, A. S. L. Gomes, and E. Sauvain, "Laser action in strongly scattering media," Nature **368**, 436–438 (1994).

[4] C. Vanneste and P. Sebbah, "Selective excitation of localized modes in active random media," Phys. Rev. Lett. **87**, 183903 (2001).

[5] H. Coles and S. Morris, "Liquid-crystal lasers," Nat. Photonics **4**, 676–685 (2010).

[6] N. Bachelard, S. Gigan, X. Noblin, and P. Sebbah, "Adaptive pumping for spectral control of random lasers," Nat. Phys. **10**, 426–431 (2014).

[7] A. Chanishvili, G. Chilaya, G. Petriashvili, R. Barberi, R. Bartolino, G. Cipparrone, A. Mazzulla, R. Gimenez, L. Oriol, and M. Pinol, "Widely tunable ultraviolet-visible liquid crystal laser," Appl. Phys. Lett. **86**, 051107 (2005).

[8] D. S. Wiersma, "The physics and applications of random lasers," Nat. Phys. **4**, 359–367 (2008).

[9] B. Xu, Z. Gao, Y. Wei, Y. Liu, X. Sun, W. Zhang, X. Wang, Z. Wang, and X. Meng, "Dynamically wavelength-tunable random lasers based on metal–organic framework particles," Nanoscale **12**, 4833–4838 (2020).

[10] S. Gottardo, R. Sapienza, P. D. García, A. Blanco, D. S. Wiersma, and C. López, "Resonance-driven random lasing," Nat. Photonics **2**, 429–432 (2008).

[11] X. Shi, W. Song, D. Guo, J. Tong, and T. Zhai, "Selectively visualizing the hidden modes in random lasers for secure communication," Laser Photonics Rev. **15**, 2100295 (2021).

[12] S. F. Haddawi, H. R. Humud, and S. M. Hamidi, "Signature of plasmonic nanoparticles in multi-wavelength low power random lasing," Opt. Laser Technol. **121**, 105770 (2020).

[13] L. Chen, Z. Liu, K. Che, Y. Bu, S. Li, Q. Zhou, H. Xu, and Z. Cai, "Thermo-switchable multi-wavelength laser emission from a dye-doped nematic liquid-crystal device," Thin Solid Films **520**, 2971–2975 (2012).

[14] J.-D. Lin, Y.-S. Zhang, J.-Y. Lee, T.-S. Mo, H.-C. Yeh, and C.-R. Lee, "Electrically tunable liquid-crystal–polymer composite laser with symmetric sandwich structure," Macromolecules **53**, 913–921 (2020).

[15] S. Gottardo, S. Cavalieri, O. Yaroshchuk, and D. S. Wiersma, "Quasi-two-dimensional diffusive random laser action," Phys. Rev. Lett. **93**, 263901 (2004).

[16] Q. Song, L. Liu, L. Xu, Y. Wu, and Z. Wang, "Electrical tunable random laser emission from a liquid-crystal infiltrated disordered planar microcavity," Opt. Lett. **34**, 298–300 (2009).

[17] S. Gao, J. Wang, W. Li, X. Yu, X. Zhang, X. Song, A. Iljin, I. Drevensek-Olenik, R. A. Rupp, and J. Xu, "Low threshold random lasing in dye-doped and strongly disordered chiral liquid crystals," Photonics Res. **8**, 338706 (2020).

[18]F. Zhang and D.-K. Yang, "Temperature dependence of pitch and twist elastic constant in a cholesteric to smectic A phase transition," Liq. Cryst. **29**, 1497–1501 (2002).

[19]J. Li, S. Gauza, and S.-T. Wu, "Temperature effect on liquid crystal refractive indices," J. Appl. Phys. **96**, 19–24 (2004).

[20]Y. Huang, Y. Zhou, C. Doyle, and S.-T. Wu, "Tuning the photonic band gap in cholesteric liquid crystals by temperature-dependent dopant solubility," Opt. Express **14**, 1236–1242 (2006).

[21]K. Funamoto, M. Ozaki, and K. Yoshino, "Discontinuous shift of lasing wavelength with temperature in cholesteric liquid crystal," Jpn. J. Appl. Phys. **42**, L1523 (2003).

[22]S. M. Morris, A. D. Ford, M. N. Pivnenko, and H. J. Coles, "Enhanced emission from liquid-crystal lasers," J. Appl. Phys. **97**, 023103 (2005).

[23]S. M. Morris, A. D. Ford, and H. J. Coles, "Removing the discontinuous shifts in emission wavelength of a chiral nematic liquid crystal laser," J. Appl. Phys. **106**, 023112 (2009).

[24]L. Cerdán, A. Costela, and I. García-Moreno, "Waveguided random lasing in red-emitting-dye-doped organic–inorganic hybrid polymer thin films," Org. Electron. **13**, 1463–1469 (2012).

[25]H. Lu, J. Hu, Y. Chu, W. Xu, L. Qiu, X. Wang, G. Zhang, J. Hu, and J. Yang, "Cholesteric liquid crystals with an electrically controllable reflection bandwidth based on ionic polymer networks and chiral ions," J. Mater. Chem. C **3**, 5406–5411 (2015).

[26]J. Xiang, Y. Li, Q. Li, D. A. Paterson, J. M. D. Storey, C. T. Imrie, and O. D. Lavrentovich, "Electrically tunable selective reflection of light from ultraviolet to visible and infrared by heliconical cholesterics," Adv. Mater. **27**, 3014–3018 (2015).

[27]H. Kim, J. Kobashi, Y. Maeda, H. Yoshida, and M. Ozaki, "Pitch-length independent threshold voltage of polymer/cholesteric liquid crystal nano-composites," Crystals **5**, 302–311 (2015).

[28]H. Kim, Y. Inoue, J. Kobashi, Y. Maeda, H. Yoshida, and M. Ozaki, "Deformation-free switching of polymer-stabilized cholesteric liquid crystals by low-temperature polymerization," Opt. Mater. Express **6**, 705–710 (2016).

[29]D. S. Wiersma and S. Cavalieri, "A temperature-tunable random laser," Nature **414**, 708–709 (2001).

[30]Y. Lu, G. L. Liu, and L. P. Lee, "High-density silver nanoparticle film with temperature-controllable interparticle spacing for a tunable surface enhanced Raman scattering substrate," Nano Lett. **5**, 5–9 (2005).

[31]Q. Yu, P. Guan, D. Qin, G. Golden, and P. M. Wallace, "Inverted size-dependence of surface-enhanced Raman scattering on gold nanohole and nanodisk arrays," Nano Lett. **8**, 1923–1928 (2008).

[32]K. H. Drexhage, "Influence of a dielectric interface on fluorescence decay time," J. Lumin. **1-2**, 693–701 (1970).

[33]K. Ray, M. H. Chowdhury, and J. R. Lakowicz, "Observation of surface plasmon-coupled emission using thin platinum films," Chem. Phys. Lett. **465**, 92–95 (2008).

[34]K. Aslan, J. R. Lakowicz, and C. D. Geddes, "Metal-enhanced fluorescence using anisotropic silver nanostructures: Critical progress to date," Anal. Bioanal. Chem. **382**, 926–933 (2005).

[35]V. M. Parfenyev and S. S. Vergeles, "Quantum theory of a spaser-based nanolaser," Opt. Express **22**, 13671–13679 (2014).

[36]R. F. Oulton, V. J. Sorger, T. Zentgraf, R.-M. Ma, C. Gladden, L. Dai, G. Bartal, and X. Zhang, "Plasmon lasers at deep subwavelength scale," Nature **461**, 629–632 (2009).

[37]X. Meng, A. V. Kildishev, K. Fujita, K. Tanaka, and V. M. Shalaev, "Wavelength-tunable spasing in the visible," Nano Lett. **13**, 4106–4112 (2013).

[38]A. Fernandez-Bravo, D. Wang, E. S. Barnard, A. Teitelboim, C. Tajon, J. Guan, G. C. Schatz, B. E. Cohen, E. M. Chan, and P. J. Schuck, "Ultralow-threshold, continuous-wave upconverting lasing from subwavelength plasmons," Nat. Mater. **18**, 1172–1176 (2019).

[39]R. Sato, J. Henzie, B. Zhang, S. Ishii, S. Murai, K. Takazawa, and Y. Takeda, "Random lasing via plasmon-induced cavitation of microbubbles," Nano Lett. **21**, 6064–6070 (2021).

[40]D. He, W. Bao, L. Long, P. Zhang, M. Jiang, and D. Zhang, "Random lasing from dye-Ag nanoparticles in polymer films: Improved lasing performance by localized surface plasmon resonance," Opt. Laser Technol. **91**, 193–196 (2017).

[41]G. Haran, "Single-molecule fluorescence spectroscopy of biomolecular folding," J. Phys.: Condens. Matter **15**, R1291–R1317 (2003).

[42]Y. Sun, S. I. Shopova, C.-S. Wu, S. Arnold, and X. Fan, "Bioinspired optofluidic FRET lasers via DNA scaffolds," Proc. Natl. Acad. Sci. U. S. A. **107**, 16039–16042 (2010).

[43]M. Cardoso Dos Santos, W. R. Algar, I. L. Medintz, and N. Hildebrandt, "Quantum dots for Förster resonance energy transfer (FRET)," TrAC, Trends Anal. Chem. **125**, 115819 (2020).

[44]B. Hellenkamp, S. Schmid, O. Doroshenko, O. Opanasyuk, R. Kühnemuth, S. Rezaei Adariani, B. Ambrose, M. Aznauryan, A. Barth, V. Birkedal, M. E. Bowen, H. Chen, T. Cordes, T. Eilert, C. Fijen, C. Gebhardt, M. Götz, G. Gouridis, E. Gratton, T. Ha, P. Hao, C. A. Hanke, A. Hartmann, J. Hendrix, L. L. Hildebrandt, V. Hirschfeld, J. Hohlbein, B. Hua, C. G. Hübner, E. Kallis, A. N. Kapanidis, J.-Y. Kim, G. Krainer, D. C. Lamb, N. K. Lee, E. A. Lemke, B. Levesque, M. Levitus, J. J. McCann, N. Naredi-Rainer, D. Nettels, T. Ngo, R. Qiu, N. C. Robb, C. Röcker, H. Sanabria, M. Schlierf, T. Schröder, B. Schuler, H. Seidel, L. Streit, J. Thurn, P. Tinnefeld, S. Tyagi, N. Vandenberk, A. M. Vera, K. R. Weninger, B. Wünsch, I. S. Yanez-Orozco, J. Michaelis, C. A. M. Seidel, T. D. Craggs, and T. Hugel, "Precision and accuracy of single-molecule FRET measurements-a multi-laboratory benchmark study," Nat. Methods **15**, 669–676 (2018).

[45]J. Hohlbein, T. D. Craggs, and T. Cordes, "Alternating-laser excitation: Single-molecule FRET and beyond," Chem. Soc. Rev. **43**, 1156–1171 (2014).

[46]V. I. Kopp, Z.-Q. Zhang, and A. Z. Genack, "Lasing in chiral photonic structures," Prog. Quantum Electron. **27**, 369–416 (2003).

[47]H. Lu, J. Xing, C. Wei, J. Xia, J. Sha, Y. Ding, G. Zhang, K. Xie, L. Qiu, and Z. Hu, "Band-gap-tailored random laser," Photonics Res. **6**, 390–395 (2018).

[48]H. Yingjuan, L. Ruiyi, L. Zaijun, S. Xiulan, G. Zhiquo, W. Guangli, and L. Junkang, "Resonance light scattering method for the detection of peanut allergen-Ara h 1 using gold nanorods prepared by improved synthesis through the use of a sodium dodecyl benzene sulfonate additive," Anal. Methods **5**, 5478–5485 (2013).

[49]H. Zong, X. Wang, X. Mu, J. Wang, and M. Sun, "Plasmon-enhanced fluorescence resonance energy transfer," Chem. Rec. **19**, 818–842 (2019).

[50]X.-C. Ma, Y. Dai, L. Yu, and B.-B. Huang, "Energy transfer in plasmonic photocatalytic composites," Light: Sci. Appl. **5**, e16017 (2016).

[51]F. Medeghini, J. Pettine, S. M. Meyer, C. J. Murphy, and D. J. Nesbitt, "Regulating and directionally controlling electron emission from gold nanorods with silica coatings," Nano Lett. **22**, 644–651 (2022).

[52]R. M. Bakker, H.-K. Yuan, Z. Liu, V. P. Drachev, A. V. Kildishev, V. M. Shalaev, R. H. Pedersen, S. Gresillon, and A. Boltasseva, "Enhanced localized fluorescence in plasmonic nanoantennae," Appl. Phys. Lett. **92**, 043101 (2008).

[53]Z. Wang, X. Meng, S. H. Choi, S. Knitter, Y. L. Kim, H. Cao, V. M. Shalaev, and A. Boltasseva, "Controlling random lasing with three-dimensional plasmonic nanorod metamaterials," Nano Lett. **16**, 2471–2477 (2016).

[54]A. S. L. Gomes, B. C. Lima, P. I. R. Pincheira, A. L. Moura, M. Gagné, E. P. Raposo, C. B. de Araújo, and R. Kashyap, "Glassy behavior in a one-dimensional continuous-wave erbium-doped random fiber laser," Phys. Rev. A **94**, 011801 (2016).